REPORT DOCUMENTATION PAGE

Form Approved
OMB No. 0704-0188

PLEASE DO NOT RETURN YOUR FORM TO THE ABOVE ADDRESS.

1. REPORT DATE *(DD-MM-YYYY)*	2. REPORT TYPE	3. DATES COVERED *(From - To)*
31102002	Proceeding	

4. TITLE AND SUBTITLE

Remote sensing of sand ripples using high-frequency backscatter

5a. CONTRACT NUMBER
N0001402WX30017

5b. GRANT NUMBER
N/A

5c. PROGRAM ELEMENT NUMBER
0602435N

6. AUTHOR(S)
Dajun Tang, Kevin L. Williams, Eric I. Thorsos, Kevin B. Briggs

5d. PROJECT NUMBER
BE-782-001

5e. TASK NUMBER

5f. WORK UNIT NUMBER
74-6626-00

7. PERFORMING ORGANIZATION NAME(S) AND ADDRESS(ES)
Naval Research Laboratory
Marine Geoacoustics Division
Stennis Space Center MS 39529

8. PERFORMING ORGANIZATION REPORT NUMBER
NRL/PP/7430-02-6

9. SPONSORING/MONITORING AGENCY NAME(S) AND ADDRESS(ES)

Office of Naval Research
800 North Quincy Street
Arlington VA 22217-5000

10. SPONSOR/MONITOR'S ACRONYM(S)
ONR

11. SPONSOR/MONITOR'S REPORT NUMBER(S)

12. DISTRIBUTION/AVAILABILITY STATEMENT
Approved for public release; distribution is unlimited

13. SUPPLEMENTARY NOTES
Oceans 2002 MTS/IEEE Conference Proceeding

14. ABSTRACT
It is critical for buried target detection via ripple scattering to know the ripple structure, e.g., the ripple height and spatial wavelength. In the present paper, backscattering data from a 300-kHz system show that ripple wavelength and height can potentially be estimated from backscattering images. Motivated by the backscatter data, we have developed a time-domain numerical model to simulate scattering of high-frequency sound by a ripple field. This model treats small-scale scatterers as Lambertian scatterers distributed randomly on the large-scale ripple field. We have found that this approach characterizes the field data well. Numerical simulations are conducted to investigate the possibility of remotely sensing bottom ripple heights and wavelength.

15. SUBJECT TERMS
buried target detection; ripple scattering; backscattering;

16. SECURITY CLASSIFICATION OF:			17. LIMITATION OF ABSTRACT	18. NUMBER OF PAGES	19a. NAME OF RESPONSIBLE PERSON
a. REPORT	b. ABSTRACT	c. THIS PAGE			Kevin B. Briggs
Unclassified	Unclassified	Unclassified	SAR	5	19b. TELEPHONE NUMBER *(Include area code)* 228-688-5518

Remote sensing of sand ripples using high-frequency backscatter

Dajun Tang, Kevin L. Williams, Eric I. Thorsos
Applied Physics Laboratory, University of Washington,
Seattle, WA 98105

Kevin B. Briggs
Seafloor Sciences Branch, Naval Research Laboratory,
Stennis Space Center, MS 39529

Abstract—**It is critical for buried target detection via ripple scattering to know the ripple structure, e.g., the ripple height and spatial wavelength. In the present paper, backscattering data from a 300-kHz system show that ripple wavelength and height can potentially be estimated from backscattering images. Motivated by the backscatter data, we have developed a time-domain numerical model to simulate scattering of high-frequency sound by a ripple field. This model treats small-scale scatterers as Lambertian scatterers distributed randomly on the large-scale ripple field. We have found that this approach characterizes the field data well. Numerical simulations are conducted to investigate the possibility of remotely sensing bottom ripple heights and wavelength.**

I. Introduction

The presence of bottom ripple fields changes high-frequency (> 10 kHz) acoustic interaction with sediments [1]. Therefore, it is critical for buried target detection at these frequencies to know the ripple structure of the sediment interface, including the ripple height and spatial wavelength. In previous work, in situ measurements of ripples were made using stereo photography and electrical conductivity [2]. Although these methods are accurate and dependable, they can only be carried out over very limited regions (on the order of 1–5 meters in length). Use of the backscatter of high-frequency sound to remotely measure the ripple field, on the other hand, can potentially cover much larger areas (on the order of 50-m-square area) and is fast. Backscattering data were taken using a 300-kHz system off the coast of Fort Walton Beach, FL, where a sand ripple field was observed and its characteristics were independently measured. The data clearly show that ripples can be observed in the backscattering strength data. Motivated by this result, we have developed a numerical model to study the possibility of inverting for the ripple field using high-frequency backscattering data.

II. Field Data

The 300-kHz backscattering data were taken at a shallow-water site off Fort Walton Beach, FL, where the ripples had a nominal peak-to-trough height of 3 cm (as measured from conductivity probes and stereo photogrammetry [2]). The acoustic system has a center frequency of 300 kHz, a bandwidth of 10 kHz, and acquires data over 360° in azimuth. The transmitter has a one-degree azimuthal beamwidth and was mounted three meters above the bottom. Details of the system can be found in [3].

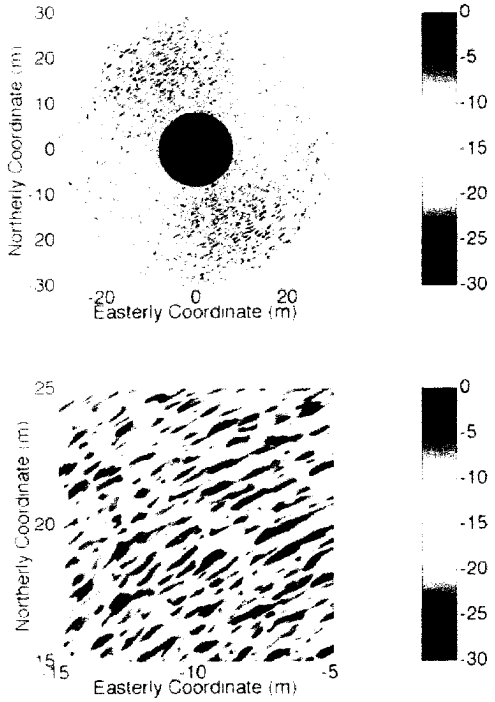

Fig. 1. Backscattering data expressed in terms of the Lambert parameter. The color scale gives the Lambert parameter in dB. The lower panel is an enlarged portion of the upper panel to show more details.

Fig. 1 shows the backscattered data expressed in terms of the Lambert parameter, which is 10 times the logarithm of the scattering cross section divided by the square of the sine of the grazing angle. The backscatter data were projected onto the bottom by relating two-way travel time to locations on the bottom. There are two points of special note in Fig. 1: first, spatial changes in scattering due to the ripple field can be seen in the second and fourth quadrants of the upper panel and in the lower panel where the sonar was oriented perpendicular to the ripples. In the first and third quadrants of the upper panel, where the sonar beam was parallel to the ripples, the ripples understandably have little effect on backscattering. Second, the data overall do not show a range dependence, or equivalently a grazing angle dependence. This is especially clear in the first and third quadrants of the

This work was supported by the Office of Naval Research MCM program and Ocean Acoustics program.

upper panel. Since the data are presented as the Lambert parameter, the lack of angular dependence indicates that the backscattering strength (10 times of the logarithm of the scattering cross section) can be well modeled by Lambert's law where the backscattering cross section is proportional to the second power of the sine of the grazing angle. It is straightforward to average the data in the first and third quadrants of the upper panel of the figure to obtain the mean Lambert parameter. This mean is about -15 dB.

III. Numerical Simulations

Based on the observations from the field data, we assume that high-frequency backscatter from the sandy sediments can be modeled by a two-scale model. In the absence of the ripples, the backscattering strength obeys Lambert's law with the Lambert parameter being -15 dB. The effect of the ripples is simply that they will change the local grazing angle and, hence, the local scattering strength. We have developed a Monte-Carlo simulation of bottom backscatter consistent with the aforementioned assumptions. The following steps are taken to arrive at the time-domain simulated pressure field:

- A patch of rough rippled seafloor is generated, which is either a deterministic sinusoidal ripple field or a random realization based on a Gaussian power spectrum with its dominant spectral component corresponding to the main ripple wavelength.
- The patch of seafloor is divided into pixels, each one smaller than a quarter of the acoustic wavelength. When the source position is specified, grazing angles relative to the flat seafloor and to the rippled seafloor are calculated. In each pixel, a random scatterer is assigned which statistically gives Lambert's backscattering strength when the backscattered intensity is ensemble averaged. Note that it is the local grazing angle (*i.e.*, the grazing angle relative to the rippled seafloor) that is used to determine the average strength of the scatterer in each pixel. In doing this step, care was taken to make sure that the scattering strength is independent of the pixel size chosen.
- Source parameters such as source strength (220 dB re: 1 μPa), transmit and receive beam patterns, depression angle, and center frequency and bandwidth are specified. In the present simulation, a windowed 32-cycle sine wave centered at 300 kHz was used.
- Ranges from the source to all pixels are calculated. The water column was assumed to have a constant sound speed of 1480 m/s. The two-way delay time for each pixel is calculated. To ensure a spatial random distribution of scatterers, we further make the scatterer location inside the pixel uniformly random.
- Contributions of the scattered pressure from each pixel are coherently added to arrive at the final backscattered pressure field.

All results reported in this paper were obtained from simulations on a one-dimensional surface with the sound beam oriented perpendicular to the ripples. Fig. 2 shows examples of the rough surface profile $f(x)$, the grazing angle, and the source beam pattern loss for a case with mean ripple wavelength of 50 cm and rms ripple height of 1 cm. Fig. 3 is the simulated backscattered pressure generated using the model. The pressure envelope demonstrates a fluctuation that is the result of the presence of the ripples given in Fig. 2. Simulations generated using this model are used as data to invert for the ripple surface in the next section.

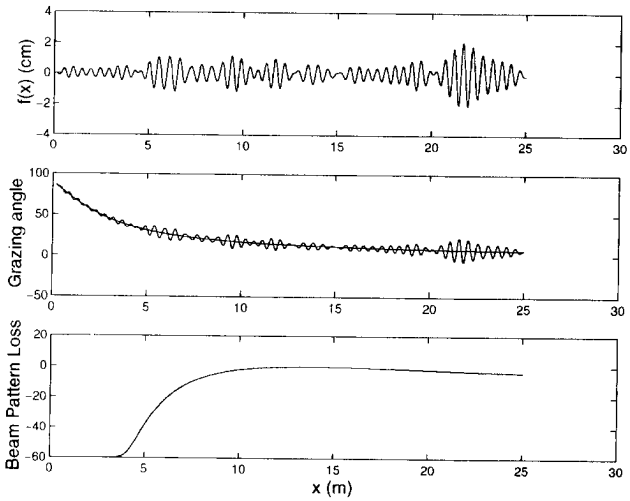

Fig. 2. One example of the rippled surface. The top panel gives the rough surface height. The middle panel shows the grazing angle in degrees: the fluctuating curve is the local grazing angle associated with the rough surface; the smooth curve is the grazing angle if the surface is flat. The bottom panel shows the source beam pattern loss in dB.

IV. Inversion Procedures

In this section two results are presented. The first is for a case where a sinusoidal ripple is used in the simulations. The second is for a case where random realizations of ripple surfaces are used. The goal is to outline the procedures for using the simulated data to invert for the ripple surfaces.

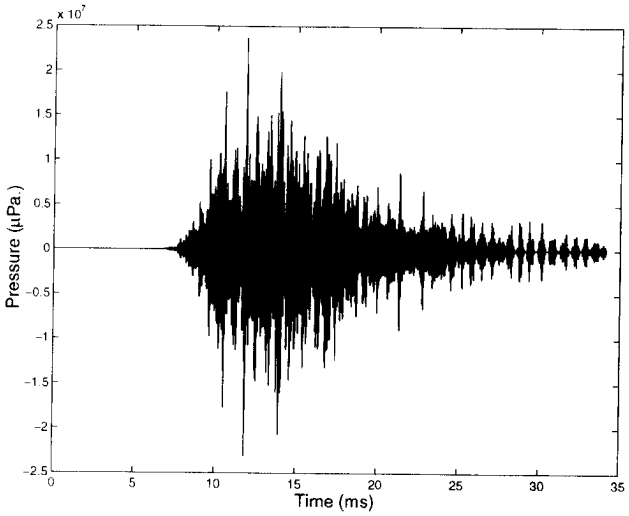

Fig. 3. Simulated pressure corresponding to the rough surface given in Fig. 2. The source level is 220 dB re 1 μPa. The frequency is 300 kHz.

In simulations with a sinusoid surface, we chose the ripple field to have a wavelength of 50 cm and amplitude of 1 cm (2 cm peak-to-peak). Fig. 4 shows backscattering strength based on an average over an ensemble of 10 realizations. The dashed curve is the theoretical scattering strength based on Lambert's law when the ripple is absent. The solid curve shows the corresponding scattering strength when the ripple is present. It is clear that when there is a ripple field, the scattering strength fluctuates around that of the flat surface with a variation greater than 20 dB. For one side of a ripple, the local grazing angle the impinging sound makes with the bottom is larger than that for the flat case, hence a larger scattering strength results. For the other side of the ripple, the local grazing angle is smaller, resulting in a much reduced scattering strength. The pluses in the figure show the results of averaging the backscattered intensity results for 10 realizations (*e.g.*, Fig. 3). By construction, when the ensemble size goes to infinity, the averaged result approaches the theoretical curve. If in practice we could get a good estimate of the scattering strength, the inversion would be relatively straightforward; one could simply relate the scattering strength to the local slope of the rough surface. However, because the ripple fields are changing from location to location, it is impractical to expect that ensemble-averaged results could be obtained. Therefore, one needs to work with data from single realizations. Fig. 5 is an example of a single realization result. Compared to the result in Fig. 4, the data show a marked increase in fluctuations, which is expected from the random nature of the simulations. The source bandwidth allows 7.5-cm resolution in range, consistent with the 32-cycle pulse used in the simulations. We have found it useful to locally average the backscattered intensity over a larger range interval to reduce the fluctuations. Fig. 6 is the result of averaging the backscattered intensity corresponding to Fig. 5 over 24-cm segments. Whereas the resulting scattering strength shows deviations when compared to the theoretical curve, the large fluctuations have been eliminated. We have not attempted to compensate for the averaging on the ripple induced variations, but this will be done in future work.

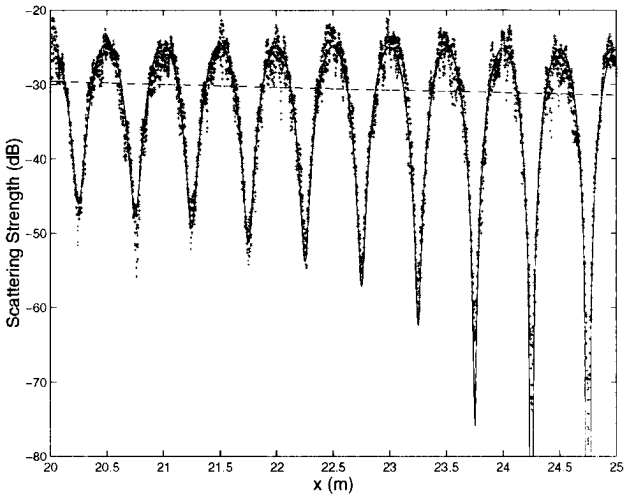

Fig. 4. Simulated scattering strength at 300 kHz. The dashed curve is the theoretical result for a flat surface, the solid curve is the theoretical result for a sinusoid ripple field, and the pluses are from simulations.

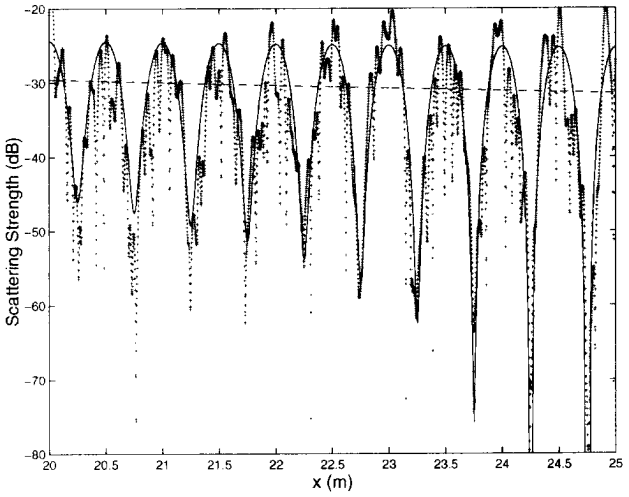

Fig. 5. Same as in Fig. 4, but the simulation is for a single realization.

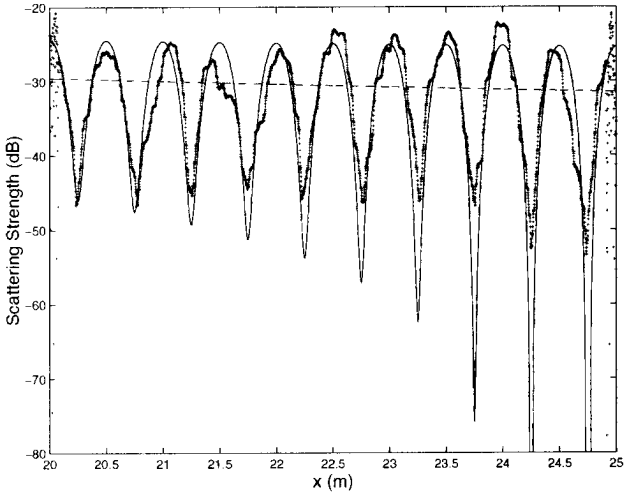

Fig. 6. Locally averaged result from single realization shown in Fig. 5.

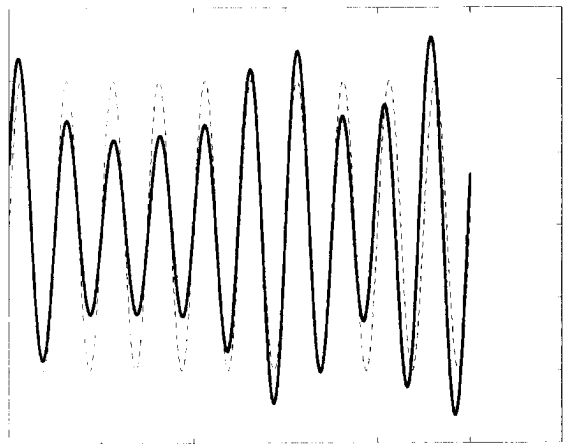

Fig. 7. Ripple surface. The dashed curve is the input sinusoid surface. The solid curve is the inverted surface based on results from Fig. 6.

When the scattering strength as a function of range is known, local grazing angles can be calculated through Lambert's law with a known Lambert parameter. The difference between the local grazing angle and the grazing angle associated with the flat surface is related to the slope of the ripple surface by simple geometry. Fig. 7 shows the inversion result for the rippled surface along with the input sinusoid surface. Note that whereas the amplitude has marked error in some regions compared to the input sinusoid, the periodicity is fairly accurate throughout the range plotted. Our calculations for this particular inversion result indicate that the mean wavelength of the inverted surface is 50.10 cm while the sinusoid wavelength is 50.00 cm. The rms height is 0.66 cm for the inverted surface and 0.707 cm for the sinusoid surface.

Now we turn our attention to cases where ripple surfaces are random, rather than sinusoidal. Here the surfaces were generated using a Gaussian power spectrum with its mean wavenumber at $2\pi/(50\text{ cm})$ and standard deviation of 10% of the mean wavenumber. Figs. 8, 9, and 10 are similar to Figs. 5, 6, and 7, respectively, except that the input ripple surface is randomly generated as described. For this set of simulations, we arrive at the same conclusions that locally smoothing the scattering strength for a single realization can lead to a fairly good reconstruction of the ripple surface as shown in Fig. 10. Here again we calculated the mean wavelength and the rms surface height of the original and inverted surfaces. The results are that the mean wavelength is 45.55 cm for the inverted surface and is 50 cm for the original surface. The rms height is 0.39 cm for the inverted surface and is 0.49 cm for the original surface. Please note these results are from a single realization.

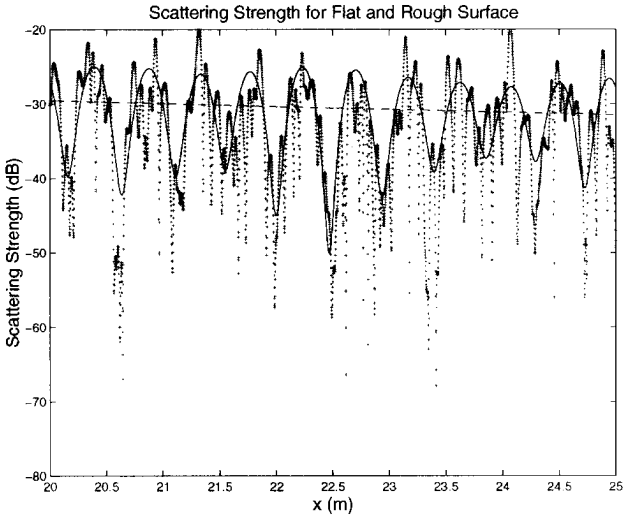

Fig. 8. Simulated scattering strength at 300 kHz. The dashed curve is for a flat surface, the solid curve is the theoretical result for a randomly generated ripple surface, and the pluses are for a single realization.

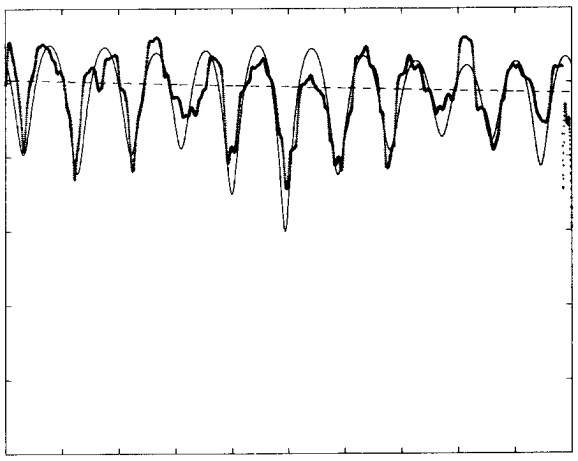

Fig. 9. Locally averaged result for the single realization shown in Fig. 8.

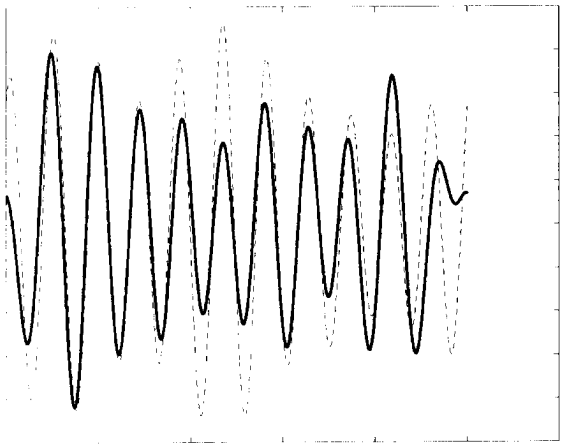

Fig. 10. Ripple surface. The dashed curve is the input rough surface. The solid curve is the inverted result based on results from Fig. 9.

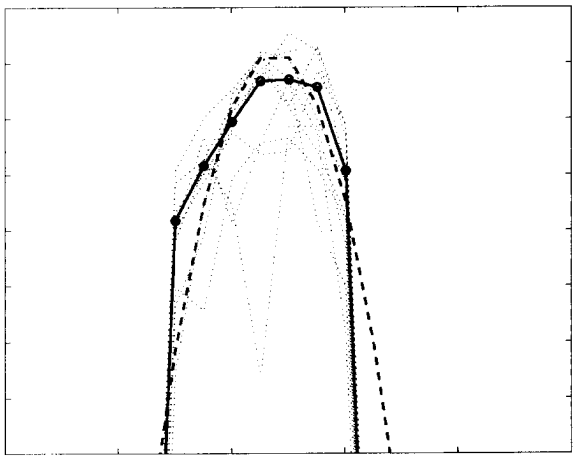

Fig. 11. Comparison of inverted mean power spectrum (solid) to the input power spectrum (dashed). The dotted curves are the 10 individual spectral estimates.

Finally, we examine the possibility of estimating the power spectrum of the ripple field from inverted surfaces. The power spectrum was calculated from 10 inverted surfaces similar to the one given in Fig. 10, and was compared to the input Gaussian power spectrum. The comparison is given in Fig. 11. The result shows that the difference in peak values between the input power spectrum and the inverted mean spectrum is less than 2 dB and the spectral widths for the two spectra are very similar.

V. Summary

High-frequency backscattering data from field measurements at the rippled sandy sediment show that the scattering strength is influenced by the presence of the ripple field through the change of local grazing angle. This modulation effect provides an opportunity to use backscatter data to invert for the ripple surface and to estimate the power spectrum of the ripple surfaces–important results for modeling the detection of buried targets. The field data also show that when a sound beam is oriented parallel to the ripples, there is no apparent effect on the backscattering strength due to the ripples. In this case, the scattering strength can be modeled by Lambert's law. Motivated by these observations, a time-domain simulation capability was developed to investigate the possibility of inverting for the ripple field and estimating its power spectrum. Preliminary results based on simulations with one-dimensional ripple surfaces indicate that such inversion can be achieved. However, the uncertainty in the power spectrum (or equivalently the rms height on the ripple) as a function of the amount of inversion data available needs to be investigated further since predictions of buried mine detection are very sensitive to this quantity [4]. Future expansion of the simulations to two-dimensional ripple surfaces is needed to assess the effect of sound impinging from various azimuth directions relative to the ripple field. Field data inversion and validation of results will be conducted in the near future.

Acknowledgments

The NRL contribution number is NRL/PP/7430—02-0006.

References

[1] J. E. Piper, K. W. Commander, E. I. Thorsos, and K. L. Williams, "Detection of buried targets using a synthetic aperture sonar," *IEEE J. Oceanic Eng.*, July, 2002 (in press).

[2] K. B. Briggs, D. Tang, and K. L. Williams, "Characterization of Interface Roughness of Rippled Sand Off Fort Walton Beach, Florida," *IEEE J. Oceanic Eng.*, July, 2002 (in press).

[3] D. R. Jackson and K. L. Williams, "High-Frequency sea-bed scattering measurements in shallow water," Proceedings of the third European conference on underwater acoustics, Vol. 1, edited by J. S. Papadakis, Heraklion, Crete (1996).

[4] D. R. Jackson, K. L. Williams, E. I. Thorsos, and S. G. Kargl, "High-frequency subcritical acoustic penetration into a sandy sediment," *IEEE J. Oceanic Eng.*, July, 2002 (in press).